Nonequilibrium Cluster Diffusion During Growth and Evaporation in Two Dimensions

Yukio Saito,[1,2] Matthieu Dufay,[2] and Olivier Pierre-Louis[2]

[1]Department of Physics, Keio University, 3-14-1 Hiyoshi, Kohoku-ku, Yokohama 223-8522, Japan
[2]LPMCN, Université de Lyon, Lyon 1, CNRS, UMR 5586; F-69622 Villeurbanne, France

(Received 3 February 2012; published 15 June 2012)

The diffusion of growing or evaporating two-dimensional clusters is investigated. At equilibrium, it is well known that the mean square displacement (MSD) of the cluster center of mass is linear in time. In nonequilibrium conditions, we find that the MSD exhibits a nonlinear time dependence, leading to three regimes: (i) during curvature-driven evaporation, the MSD shows a square-root singularity close to the collapse time; (ii) in slow growth or evaporation, the dynamics is in the Edwards-Wilkinson universality class, and the MSD shows a logarithmic behavior; (iii) far from equilibrium, the dynamics belongs to the Kardar-Parisi-Zhang universality class and the MSD shows a power-law behavior with a characteristic exponent 1/3. These results agree with kinetic Monte Carlo simulations, and can be generalized to other universality classes.

DOI: 10.1103/PhysRevLett.108.245504 PACS numbers: 81.10.Aj, 05.40.−a, 68.35.Ct

Two-dimensional clusters with fluctuating edges (sometimes called droplets, islands, or aggregates) have been observed in many different systems such as monolayer islands on crystal surfaces [1,2]; domains in magnetic thin films [3,4]; droplets in turbulent liquid crystal films [5]; or bacteria, cell, and fungi colonies [6–8]. Many theoretical studies of two-dimensional clusters have focused on the analysis of edge fluctuations and their classification into roughening universality classes in equilibrium and nonequilibrium conditions [9–12]. However, edge fluctuations also induce the diffusion of the cluster center of mass. While the equilibrium diffusion of clusters has been studied in detail [13–15], there is, to our knowledge, no systematic study of cluster diffusion in nonequilibrium conditions. In this Letter, we discuss the nonequilibrium diffusion of 2D clusters during evaporation or growth. We provide converging analytical and kinetic Monte Carlo (KMC) simulation evidences, which show that the mean square displacement (MSD) of isotropic and anisotropic clusters exhibits a nonlinear dependence in time. We find four regimes: (i) In equilibrium, the MSD is linear in time. (ii) At saturation, the cluster evaporates via curvature-driven motion, and the MSD exhibits a $\sim 1-(1-t/t_{\rm col})^{1/2}$ behavior where $t_{\rm col}$ is the collapse time. (iii) In close-to-equilibrium growth or evaporation, interface fluctuations exhibit Edwards-Wilkinson (EW) scaling [16], and the MSD increases logarithmically with time. (iv) Far from equilibrium, the MSD exhibits a behavior attributed to Kardar-Parisi-Zhang (KPZ) scaling [17]: initially proportional to $t^{4/3}$, and crossing over to $t^{1/3}$ in growth, or to $\sim 1-(1-t/t_{\rm col})^{1/3}$ in evaporation. Our results can easily be extended to other universality classes, such as those encountered in cell colonies [7], or crystal growth with conserved dynamics [18,19].

We exemplify our results using KMC simulations on a square lattice with lattice parameter a_0, and nearest-neighbor bonds with an energy J. Such a model applies both for monolayer islands on crystal surfaces or for magnetic systems of the Ising type under an external field. In the following we use the language of atoms for clarity. We consider standard attachment-detachment limited dynamics [13]. Atoms are attached to the periphery of the cluster with the rate $\nu_0 e^{-\Delta\mu/k_BT}$, where ν_0 is an attempt frequency, $\Delta\mu$ accounts for the chemical potential difference between the bulk solid and the surrounding gas, and k_BT is the thermal energy. We work at $T = 0.2J/k_B$ lower than the Ising critical temperature $T_c \approx 0.567J/k_B$. Atoms at the solid-gas interface may detach with the rate $\nu_0 e^{-(n-2)J/k_BT}$, where n is the number of nearest-neighbor bonds to be broken by detachment. Hence, at saturation when $\Delta\mu = 0$ attachment and detachment are balanced at kink sites with $n = 2$, and a straight interface is in equilibrium with the vapor. However, equilibrium for a cluster of N atoms is reached for $\Delta\mu = \Delta\mu_c > 0$, with $\Delta\mu_c \sim N^{-1/2}$. More precisely from the Gibbs-Thomson formula $\Delta\mu_c = \Omega\tilde{\gamma}(\theta)\kappa$, where θ is the edge orientation, $\Omega = a_0^2$, and $\kappa \sim N^{-1/2}$ is the local edge curvature, $\tilde{\gamma}(\theta) = \gamma(\theta) + \gamma''(\theta)$ with $\gamma(\theta)$ the edge free energy. Note that here equilibrium is an unstable fixed point (see, e.g., Ref. [18]): Due to fluctuations islands will ultimately grow or evaporate with equal probabilities.

At saturation when $\Delta\mu = 0$, clusters evaporate with a roughly circular shape at all times as shown in Fig. 1(a). However, clusters become square during growth with $\Delta\mu > \Delta\mu_c$ or evaporation with $\Delta\mu < 0$, with sides along the (10) or (11) direction, respectively. In addition to these shape changes, the island center of mass exhibits Brownian diffusion [Fig. 1(b)]. This diffusion is a consequence of the randomness of the attachment-detachment process at the edge. At equilibrium $\Delta\mu = \Delta\mu_c$, the MSD of the cluster center of mass is expected to be linear in time [13–15]. The MSD in Fig. 1(b) appears to be slower than linear in

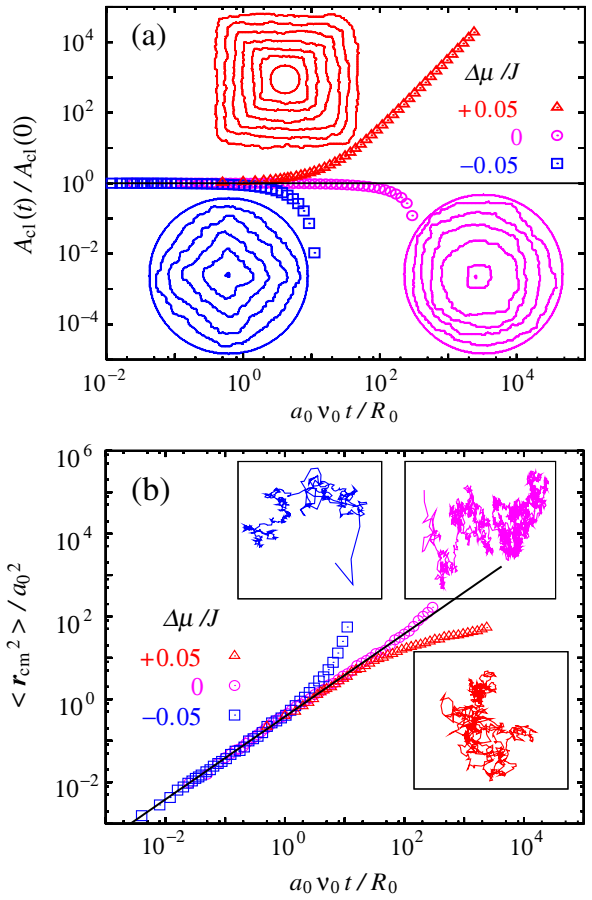

FIG. 1 (color online). KMC simulations with $k_BT = 0.2J$. (a) Cluster area $A_{cl}(t)$ averaged over 100 samples as a function of time t. (b) Mean square displacement averaged over 100 samples as a function of time. Three cases are shown: growth with chemical potential $\Delta\mu = 0.05J$ and initial radius $R_0 = 20a_0$; saturation with $\Delta\mu = 0$ and $R_0 = 400a_0$; evaporation with $\Delta\mu = -0.05J$ and $R_0 = 2500a_0$. In evaporation and at saturation, the cluster area $A_{cl}(t)$ decreases and the MSD is faster than linear, while in growth, $A_{cl}(t)$ increases and the MSD is slower than linear. Insets indicate typical shapes in (a), and trajectories of the cluster center of mass in (b).

growth, and faster than linear in evaporation. Such a tendency can be understood intuitively as a consequence of the decrease of cluster diffusion with increasing size. In the following, we present a general framework to derive the MSD from edge fluctuations. This framework provides a good description of our KMC simulations, and extends to systems with other anisotropies and other universality classes.

We describe edge fluctuations by means of a generic Langevin equation for the normal velocity v_n, with a deterministic part v_d and a stochastic part η:

$$v_n(s,t) = v_d[\{\partial_s^p \theta(s,t),\, p \geq 0\}] + \eta(s,t), \qquad (1)$$

where s is the edge arclength. The correlations of η will be specified later. Because of translational invariance, v_d cannot directly depend on the edge position $\boldsymbol{r}(s,t)$, but may depend on its orientation $\theta(s,t)$, on the local curvature $\kappa(s,t) = \partial_s\theta(s,t)$, and on higher order derivatives $\partial_s^p\theta(s,t)$, with arbitrary large p.

The velocity of the cluster center of mass $\boldsymbol{r}_{\text{c.m.}}(t)$ is then written as a function of v_n (see Supplementary Material [20]): $\partial_t \boldsymbol{r}_{\text{c.m.}}(t) = \boldsymbol{I}(v_n,t)/A_{cl}(t)$. Here, $A_{cl}(t)$ is the cluster area, and for any function $v(s,t)$, we define

$$\boldsymbol{I}(v,t) = \oint ds\, v(s,t)\boldsymbol{R}(s,t), \qquad (2)$$

where $\boldsymbol{R}(s,t) = \boldsymbol{r}(s,t) - \boldsymbol{r}_{\text{c.m.}}(t)$ characterizes the island shape. Of course, in a stationary state where $v_d(s,t)$ vanishes identically, one has $\boldsymbol{I}(v_d,t) = 0$. We shall show in the following that in nonequilibrium situations such as growth or evaporation and for isotropic dynamics, $\boldsymbol{I}(v_d,t)$ also vanishes to linear order in the noise amplitude. Isotropy means that v_d does not depend on θ, and we may write $v_d = f[\{\partial_s^p\theta,\, p \geq 1\}]$. In the referential where the center of mass is at the origin, we use the polar angle ϕ, and define $\boldsymbol{R}(s,t) = R(\phi,t)\hat{\boldsymbol{e}}_r(\phi)$, where $\hat{\boldsymbol{e}}_r(\phi)$ is the radial unit vector. Since the dynamics are isotropic, the average shape is a circle of radius $\bar{R}(t) = \langle R(\phi,t)\rangle$, and by symmetry $\langle \boldsymbol{I}(v_d,t)\rangle$ trivially vanishes. We also assume that the shape evolution of the cluster is morphologically stable, leading to small fluctuations around the average shape: $\rho(\phi,t) = R(\phi,t) - \bar{R}(t) \ll \bar{R}(t)$. To linear order in $\rho(\phi,t)$,

$$\boldsymbol{I}(v_d,t) = 2f_0\bar{R}(t)\boldsymbol{\epsilon}_0 + \sum_{p=1}^{\infty}(-1)^p f_p \bar{R}(t)^{1-p}\boldsymbol{\epsilon}_{p+1},$$

where $\boldsymbol{\epsilon}_p = \int d\phi\,\rho(\phi)\partial_\phi^p\hat{\boldsymbol{e}}_r(\phi)$, $f_0 = f[\{\bar{R}(t)^{-1},0,0,\ldots\}]$, and for $p \geq 1$: $f_p = \partial_{\partial_s^p\theta} f[\{\bar{R}(t)^{-1},0,0,\ldots\}]$. The fact that the center of mass is at the origin of our reference frame implies $\int d\phi R(\phi,t)^3\hat{\boldsymbol{e}}_r(\phi) = \boldsymbol{0}$. To first order in ρ, this latter relation leads to $\boldsymbol{\epsilon}_p = 0$ for all p's, and finally $\boldsymbol{I}(v_d,t) = \boldsymbol{0}$.

Since $\boldsymbol{I}(v_d,t)$ vanishes, only the stochastic contribution $\boldsymbol{I}(\eta,t)$ remains in Eq. (2) for steady states and isotropic dynamics. Finally, in the limit of small fluctuations, we obtain to leading order in the noise amplitude:

$$\langle \boldsymbol{r}_{\text{c.m.}}^2(t)\rangle = \int_0^t \frac{dt_1}{\langle A_1\rangle}\int_0^t \frac{dt_2}{\langle A_2\rangle}\oint ds_1 \oint ds_2 \langle \eta_1\eta_2\rangle\langle \boldsymbol{R}_1\rangle\cdot\langle \boldsymbol{R}_2\rangle, \qquad (3)$$

where $A_i = A_{cl}(t_i)$, $\eta_i = \eta(s_i,t_i)$, and $\boldsymbol{R}_i = \boldsymbol{R}(s_i,t_i)$. In order to discuss the KMC simulation results, we also need to describe anisotropic facetted shapes in growth or evaporation. Since the discussion of Eq. (3) for facetted shapes is lengthy, we shall not present it within this Letter. Here, we simply assume that Eq. (3) also applies to facetted shapes. In the following, we show that Eq. (3) provides good agreement with our KMC simulations.

Close to equilibrium, linearized dynamics is expected to provide an accurate description of KMC:

$$v_d = K(\theta)\left(\frac{\Delta\mu}{k_BT} - \Gamma(\theta)\kappa\right). \quad (4)$$

Here, $K(\theta)$ is a kinetic coefficient, and $\Gamma(\theta) = \Omega\tilde{\gamma}(\theta)/k_BT$. Furthermore, the fluctuation-dissipation relation imposes the noise amplitude:

$$\langle\eta(s_1,t_1)\eta(s_2,t_2)\rangle = 2\Omega K(\theta)\delta(s_2-s_1)\delta(t_2-t_1). \quad (5)$$

Let us first consider the equilibrium case, where $\Delta\mu/k_BT = \Gamma\kappa$. The Wulff construction [18,21] provides the equilibrium shape $\langle R(\phi)\rangle = \bar{R}\,\tilde{R}(\phi)$, where $\bar{R}$ is the average cluster radius, and $\tilde{R}(\phi)$ is a normalized shape function. Using Eqs. (3) and (5), we recover a MSD proportional to time, and the diffusion constant of an anisotropic cluster at equilibrium is

$$D_{\text{c.m.}} = \frac{\langle \boldsymbol{r}^2_{\text{c.m.}}(t)\rangle}{4t} = \frac{2\Omega}{\bar{R}}\left[\frac{\int d\tilde{s}\,\tilde{R}(\phi)^2 K(\theta(\phi))}{[\int d\phi \tilde{R}(\phi)^2]^2}\right], \quad (6)$$

where $d\tilde{s} = d\phi[\tilde{R}(\phi)^2 + \tilde{R}'(\phi)^2]^{1/2}$. We recover the result of isotropic circular clusters with radius R [13] $D^{\bigcirc}_{\text{c.m.}} = \Omega K/\pi R$, where $K(\theta) = K$ for all θ's. For a square cluster of side length $2L$, one finds $D^{\square}_{\text{c.m.}} = \Omega K_\sigma/3L$, where $K(\theta) = K_\sigma$ on the four equivalent edges.

We now investigate the nonequilibrium case where the cluster size is changing. We begin with the special case of an isotropic circular cluster of radius $\bar{R}(t) = \langle|\boldsymbol{R}(s,t)|\rangle$. The deterministic solution of Eq. (4) reads

$$\bar{R}(t) - R_0 + R_c \ln\left[\frac{\bar{R}(t)-R_c}{R_0-R_c}\right] = K\frac{\Delta\mu}{k_BT}t, \quad (7)$$

where $R_0 = \bar{R}(t=0)$ and $R_c = \Gamma k_BT/\Delta\mu$. From Eq. (3), the MSD reads:

$$\langle \boldsymbol{r}^2_{\text{c.m.}}(t)\rangle = \frac{4\Omega}{\pi}\frac{k_BT}{\Delta\mu}\ln\left[\frac{\bar{R}(t)-R_c}{R_0-R_c}\right]. \quad (8)$$

There are three major regimes. First, when $\Delta\mu > 0$ and $R_0 = R_c$, the cluster is in equilibrium, i.e., $\bar{R} = R_c$ and $\Delta\mu = \Delta\mu_c \equiv \Omega\gamma/(k_BTR_0)$. This case was discussed above, and $\langle \boldsymbol{r}^2_{\text{c.m.}}(t)\rangle = 4D^{\bigcirc}_{\text{c.m.}}t$.

In the second limit, $\bar{R}(t) \ll |R_c|$, Eqs. (7) and (8) reduce to the saturation case corresponding to $\Delta\mu \to 0$ in the simulations. The clusters shrink, driven by the chemical potential excess of the curved edge. Clusters are roughly circular during the whole evolution in KMC simulations [see Fig. 1(a)], so that our circular shape assumption is valid. In this limit, Eq. (7) reads $\bar{R}(t) = R_0(1 - t/t_{\text{col}})^{1/2}$, where $t_{\text{col}} = R_0^2/2\Gamma K$ is the collapse time. This law is in good agreement with the simulation results and allows one to extract $\Gamma K = 0.60a_0^2\nu_0$. An exact expression is known for $\tilde{\gamma}$ [22], leading to $\tilde{\gamma} \approx 0.49J/a_0$ when averaging over all orientations, so that one may extract $K \approx 0.24a_0\nu_0$. From Eq. (8), the MSD now reads

$$\langle \boldsymbol{r}^2_{\text{c.m.}}(t)\rangle = \frac{4\Omega R_0}{\pi\Gamma}[1 - (1 - t/t_{\text{col}})^{1/2}], \quad (9)$$

which exhibits a square-root singularity, but does not diverge at the collapse time t_{col}. This is confirmed by the KMC simulations in Fig. 2(a). At short times $t \ll t_{\text{col}}$, Eq. (9) reduces to the equilibrium behavior $\langle \boldsymbol{r}^2_{\text{c.m.}}(t)\rangle = 4D^{\bigcirc}_{\text{c.m.}}t$. In KMC simulations, one finds $\langle \boldsymbol{r}^2_{\text{c.m.}}(t)\rangle \approx 0.38t\nu_0a_0^3/R_0$ at short times, leading to $K \approx 0.30a_0\nu_0$. With this kinetic coefficient, we obtain a good agreement between Eq. (9) and the KMC results for various initial radii R_0, as shown in Fig. 2(a). The 20% discrepancy between the values of K obtained from the deterministic evolution and from the MSD could be a consequence of the assumption of isotropy for $\tilde{\gamma}$ and K.

When $\bar{R}(t) \gg |R_c|$, we obtain a third regime, corresponding to $|\Delta\mu| \gg \Delta\mu_c \equiv \Omega\gamma/(k_BTR_0)$, i.e., growth or evaporation with negligible capillary effects. The radius varies linearly in time $\bar{R}(t) = R_0 + Vt$ with $V = K(\Delta\mu/k_BT)$, and from Eq. (8)

$$\langle \boldsymbol{r}^2_{\text{c.m.}}(t)\rangle = \frac{4\Omega}{\pi}\frac{k_BT}{\Delta\mu}\ln\left[1 + \frac{V}{R_0}t\right]. \quad (10)$$

However, clusters are square in growth or evaporation [see Fig. 1(a)]. This shape anisotropy is controlled by the

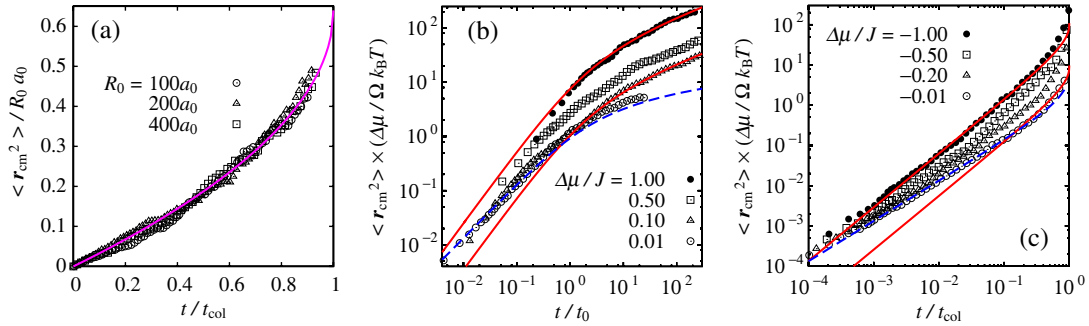

FIG. 2 (color online). Nonequilibrium MSD of two-dimensional clusters averaged over 100 samples. (a) Saturation case at $\Delta\mu = 0$ for various initial radii R_0. The solid line represents Eq. (9). (b) Growth with $L_0 = 10a_0$, except for $\Delta\mu = 0.01J$, where $L_0 = 100a_0$, and (c) evaporation with initial size $L_0 = 1768a_0$. The dashed (blue) line represents the close-to-equilibrium model, Eq. (11), and the solid (red) lines represent the far-from-equilibrium model, Eq. (17), with the noise amplitude B_f as a fitting parameter.

anisotropy of $K(\theta)$, as discussed initially by Frank [18,21]. In order to keep the same average shape at all times, we have started simulations from a square shape with (10) and (11) edges for growth and evaporation, respectively. The distance between the center and the edges L then obeys $L = L_0 + K_\sigma(\Delta\mu/k_BT)t = L_0 + V_\sigma t$, where $L_0 = L(t = 0)$, and σ is (10) for growth or (11) for evaporation. In KMC simulations, we find $V_{(10)} \approx 0.085 a_0\nu_0$ at $\Delta\mu = 0.01J$, and $V_{(11)} \approx -0.018 a_0\nu_0$ at $\Delta\mu = -0.01J$, leading to $K_{(10)} = 0.17 a_0\nu_0$ and $K_{(11)} = 0.36 a_0\nu_0$. Note that $K_{(10)} < K < K_{(11)}$, as expected [18,21], since the slowest (10) and fastest (11) edges should be present in growth and in evaporation, respectively. From Eq. (3), we obtain logarithmic behavior of the MSD of square clusters similar to Eq. (10):

$$\langle \boldsymbol{r}^2_{\text{c.m.}}(t)\rangle = \frac{4\Omega}{3}\frac{k_BT}{\Delta\mu}\ln\left[1 + \frac{V_\sigma}{L_0}t\right]. \tag{11}$$

As shown in Figs. 2(b) and 2(c) the KMC simulation results are in quantitative agreement with Eq. (11) in the limit of small $|\Delta\mu|/k_BT$.

However, when $|\Delta\mu|/k_BT$ increases, the MSD deviates from Eq. (11). Indeed, far from equilibrium, one expects dynamical roughening of the edge within the one-dimensional KPZ universality class [17]. A detailed theoretical analysis of the growth of clusters within the KPZ regime is discussed in several recent papers [9–12]. However, these studies only focus on the edge roughness, and do not consider cluster diffusion. Here we would like to capture the MSD behavior within the nonlinear KPZ regime with Eq. (3). Since Eq. (3) is valid for linear evolution equations only, we need to design a linear ansatz which is able to reproduce the KPZ scaling behavior. We then plug this ansatz in Eq. (3) to obtain the MSD.

We first consider isotropic dynamics, and define the Fourier coefficients of $\rho(\phi, t)$ with respect to ϕ as $\rho_n(t)$, where n is an integer. We postulate a linear evolution equation with v_d nonlocal in space, and noise correlations that are nonlocal in time:

$$\partial_t\rho_n(t) = -\frac{A_{\text{iso}}}{\bar{R}(t)^a}|n^2 - 1|^{a/2}\rho_n(t) + \frac{\tilde{\eta}_n(t)}{\bar{R}(t)^{1/2}}, \tag{12}$$

$$\langle \tilde{\eta}_n(t)\tilde{\eta}_{n'}(t')\rangle = 2\pi\delta_{n+n'}\frac{bB_{\text{iso}}}{|t - t'|^{1-b}}, \tag{13}$$

where A_{iso} and B_{iso} are constants. The case $a = 2$, $b = 0$ reproduces exactly the close-to-equilibrium behavior obtained by linearizing Eq. (4) for small ρ, and corresponds to EW scaling, with dynamic exponent $z = 2$ and roughness exponent $\alpha = 1/2$ [16]. In general, comparing the asymptotics for the dynamical structure factor of ρ [23] with those expected for a system with roughening exponents z and α, we obtain $a = z$ and $b = (2\alpha + 1)/z - 1$. Therefore, KPZ scaling with $z = 3/2$ and $\alpha = 1/2$ [17] corresponds to $a = 3/2$ and $b = 1/3$. Assuming a constant velocity for the average radius $\bar{R}(t) = R_0 + Vt$, the MSD is evaluated from Eq. (3) leading to

$$\langle \boldsymbol{r}^2_{\text{c.m.}}(t)\rangle = \frac{B_{\text{iso}}}{R_0}|t_0|^{b+1}\Lambda^b_\chi[t/|t_0|],$$
$$\Lambda^b_\chi[\tau] = \frac{2b}{\pi}\int_0^\tau d\tau_1\int_0^\tau d\tau_2\frac{1}{u_1^{1/2}u_2^{1/2}|\tau_1 - \tau_2|^{1-b}}, \tag{14}$$

where $\chi = +1$ in growth and -1 in evaporation, $u_i = 1 + \chi\tau_i$, and $t_0 = R_0/V$. In the close-to-equilibrium regime corresponding to the EW universality class with $b = 0$, we recover Eq. (10). Far from equilibrium with large $|\Delta\mu|/k_BT$, we expect KPZ scaling, leading to $\langle \boldsymbol{r}^2_{\text{c.m.}}(t)\rangle \sim t^{4/3}$ at $t \ll |t_0|$ both for growth and for evaporation. One finds $\langle \boldsymbol{r}^2_{\text{c.m.}}(t)\rangle \sim t^{1/3}$ in growth at $t \gg t_0$, and $\langle \boldsymbol{r}^2_{\text{c.m.}}(t)\rangle \sim 1 - (1 - t/t_{\text{col}})^{1/3}$ in evaporation close to the collapse.

One may design a linear model for facetted clusters along the same lines. Defining the interface deviation $\zeta(x, t)$ at the position x along a given facet, we postulate the dynamics of the Fourier transform $\zeta_q(t)$ as

$$\partial_t\zeta_q(t) = -A_f|q|^a\zeta_q(t) + \eta_q(t), \tag{15}$$

$$\langle \eta_q(t)\eta_{q'}(t')\rangle = 2\pi\delta(q + q')\frac{bB_f}{|t - t'|^{1-b}}, \tag{16}$$

where A_f and B_f are constants, and we assume that the noise is not correlated between different facets. From Eq. (3), we then find for a regular polygon with n facets

$$\langle \boldsymbol{r}^2_{\text{c.m.}}(t)\rangle = \frac{B_f}{L_0}|t_0|^{b+1}\Xi^b_\chi[t/|t_0|],$$
$$\Xi^b_\chi[\tau] = \frac{2b}{\pi_n}\int_0^\tau d\tau_1\int_0^\tau d\tau_2 \times\frac{\min[u_1^2u_2, u_2^2u_1] + \frac{\pi_n^3}{3n^2}\min[u_1^3, u_2^3]}{u_1^2u_2^2|\tau_1 - \tau_2|^{1-b}}, \tag{17}$$

where $\pi_n = n\tan[\pi/n]$. Once again, we recover the EW result, Eq. (11), for $n = 4$ and $b = 0$. In the KPZ regime, we find the same exponents as in the isotropic case. Note that growth and evaporation scaling functions are related via $\Lambda^b_-(\tau) = (1 - \tau)^b\Lambda^b_+[\tau/(1 - \tau)]$, and $\Xi^b_-(\tau) = (1 - \tau)^b\Xi^b_+[\tau/(1 - \tau)]$.

The scaling function Ξ^b_χ, with the noise amplitude B_f as a free fitting parameter yields good agreement with KMC simulations in far-from-equilibrium growth as shown in Fig. 2(b), indicating that we have reached the KPZ regime. In addition, our results with $\Delta\mu = 0.1J$ in Fig. 2(b) suggest a crossover from EW scaling at short times to KPZ at long times. The agreement of the linear model with KMC simulations in evaporation is good at short times, but poorer in the final stages, as shown in Fig. 2(c). Since this discrepancy appears for $L \gg \Gamma$ it cannot be attributed to capillary effects, but it could be related to nontrivial contributions of the corners not included in our model.

In conclusion, we have discussed the nonequilibrium diffusion of growing or evaporating isotropic or square clusters with attachment-detachment dynamics. Other cases with different roughening exponents can also be considered within our linear ansatz, Eqs. (14) and (17), leading to a MSD $\sim t^{1+b}$ at short times, and $\sim t^b$ or $\sim 1 - (1 - t/t_{\mathrm{col}})^b$ at long times during growth or evaporation, respectively. As an example, the diffusion of atoms along the edges is known to change the equilibrium [13] and nonequilibrium [16,18] values of z and α, and should lead to different values of b. Furthermore, our work suggests the measurement of the MSD as a simpler way to determine the universality class, while previous studies relied on the spatiotemporal analysis of edge fluctuations, involving refined tracking of the moving edge. We thus hope that our results will motivate experiments to measure the MSD of clusters in a wide range of experimental systems, from magnetic domains to cell colonies [1–8].

We acknowledge support from CNRS and JSPS, and from a DéFiS ANR-PNANO grant.

[1] K. Thürmer, J. E. Reutt-Robey, E. D. Williams, M. Uwaha, A. Emundts, and H. P. Bonzel, Phys. Rev. Lett. **87**, 186102 (2001).
[2] T. Michely and J. Krug, *Islands, Mounds, and Atoms* (Springer, New York, 2004).
[3] K.-W. Moon, J.-C. Lee, S.-G. Je, K.-S. Lee, K.-H. Shin, and S.-B. Choe, Appl. Phys. Express **4**, 043004 (2011).
[4] L. Krusin-Elbaum, T. Shibauchi, B. Argyle, L. Gignac, and D. Weller, Nature (London) **410**, 444 (2001).
[5] K. A. Takeuchi and M. Sano, Phys. Rev. Lett. **104**, 230601 (2010).
[6] E. Ben-Jacob, O. Schochet, A. Tenenbaum, I. Cohen, A. Czirók and T. Vicsek, Nature (London) **368**, 46 (1994).
[7] M. A. C. Huergo, M. A. Pasquale, P. H. González, A. E. Bolzán, and A. J. Arvia, Phys. Rev. E **84**, 021917 (2011).
[8] S. Matsuura and S. Miyazima, Physica (Amsterdam) **191A**, 30 (1992).
[9] C. Escudero, Phys. Rev. Lett. **100**, 116101 (2008).
[10] J. Krug, Phys. Rev. Lett. **102**, 139601 (2009).
[11] S. B. Singha, J. Stat. Mech. (2005) P08006.
[12] T. Sasamoto and H. Spohn, Phys. Rev. Lett. **104**, 230602 (2010).
[13] S. V. Khare, N. C. Bartelt, and T. L. Einstein, Phys. Rev. Lett. **75**, 2148 (1995).
[14] W. W. Pai, A. K. Swan, Z. Zhang, and J. F. Wendelken, Phys. Rev. Lett. **79**, 3210 (1997).
[15] O. Pierre-Louis, Phys. Rev. Lett. **87**, 106104 (2001).
[16] A. Barabási and H. Stanley, *Fractal Concepts in Surface Growth* (Cambridge University Press, Cambridge, 1996).
[17] M. Kardar, G. Parisi, and Y.-C. Zhang, Phys. Rev. Lett. **56**, 889 (1986).
[18] A. Pimpinelli and J. Villain, *Physics of Crystal Growth* (Cambridge University Press, Cambridge, 1998).
[19] Z.-W. Lai and S. Das Sarma, Phys. Rev. Lett. **66**, 2348 (1991).
[20] See Supplemental Material at http://link.aps.org/supplemental/10.1103/PhysRevLett.108.245504 for a detailed derivation.
[21] Y. Saito, *Statistical Physics of Crystal Growth* (World Scientific, Singapore, 1996).
[22] C. Rottman and M. Wortis, Phys. Rev. B **24**, 6274 (1981).
[23] O. Pierre-Louis and Y. Saito (to be published).